inorganics

MDPI

Article

Structural and Antimicrobial Investigation of Some New Nanoparticles Mixed Ligands Metal Complexes of Ethyl 6-Amino-4-(4-chlorophenyl)-5-cyano-2-methyl-4H-pyran-3-carboxylate in Presence of 1,10-Phenanthroline

Mohamed S. El-Attar [1], Sadeek A. Sadeek [1], Hassan A. El-Sayed [1], Heba M. Kamal [1] and Hazem S. Elshafie [2,*]

[1] Department of Chemistry, Faculty of Science, Zagazig University, Zagazig 44519, Egypt; mselattar@zu.edu.eg (M.S.E.-A.); s_sadeek@zu.edu.eg (S.A.S.); hasanneg@zu.edu.eg (H.A.E.-S.); hm.abdelaaty019@science.zu.edu.eg (H.M.K.)

[2] School of Agricultural, Forestry, Food and Environmental Sciences, University of Basilicata, Viale dell'Ateneo Lucano 10, 85100 Potenza, Italy

* Correspondence: hazem.elshafie@unibas.it; Tel.: +39-0971-205498; Fax: +39-0971-205503

Abstract: A new series of some biologically active Cr(III), Fe(III), Co(II), Ni(II), Cu(II), and Zn(II) complexes was synthesized from the reaction of Ethyl 6-amino-4-(4-chlorophenyl)-5-cyano-2-methyl-4H-pyran-3-carboxylate **(L)** with the previous biological metals in the presence of 1,10-phenanthroline monohydrate (**Phen**). The structures of the obtained **L** along with their complexes were authenticated by different analytical and spectral techniques. The data prove that **L** chelates with all metal ions as bidentate through the nitrogen of the amino group and the nitrogen of the cyano group. Furthermore, **Phen** chelated with metal ions via two nitrogen atoms. The molar conductance values reflect that all complexes are electrolyte, confirming the 1:3 electrolytic natures for trivalent metal ions and 1:2 electrolytic for bivalent metal ions. The thermal stability and the general thermal decomposition pathways of metal complexes, **L,** and **Phen** were evaluating according to the thermogravimetric technique. The activation thermodynamic parameters were estimated from TG curves by utilizing Horowitz–Metzger (HM) and Coats–Redfern (CR) techniques. Powder X-ray diffraction (XRD) analysis proved that **L**, Cu(II), and Zn(II) compounds have a crystalline nature, whereas, Cr(III), Fe(III), Co(II), and Ni(II) complexes are semicrystalline. The investigated compounds were examined in vitro for their antimicrobial activity towards G(+ve) Staphylococcus aureus and Bacillus subtilis and G(−ve) Escherichia coli and Pseudomonas aeruginosa bacteria, and two fungi: Candida albicans and Aspergillus flavus. According to the findings, the Co(II) complex has a significant efficiency toward bacteria, additionally, Cr(III) complex is highly significant towards fungal strains.

Keywords: nanoparticles; spectroscopy; XRD; DTA; G(+ve) and G(−ve) bacteria

check for updates

Citation: El-Attar, M.S.; Sadeek, S.A.; El-Sayed, H.A.; Kamal, H.M.; Elshafie, H.S. Structural and Antimicrobial Investigation of Some New Nanoparticles Mixed Ligands Metal Complexes of Ethyl 6-Amino-4-(4-chlorophenyl)-5-cyano-2-methyl-4H-pyran-3-carboxylate in Presence of 1,10-Phenanthroline. *Inorganics* **2023**, *11*, 220. https://doi.org/10.3390/inorganics11050220

Academic Editor: Claudio Pettinari

Received: 14 April 2023
Revised: 16 May 2023
Accepted: 17 May 2023
Published: 20 May 2023

1. Introduction

Pyrans are heterocyclic components found in many natural substances, including alkaloids, carbohydrates, pheromones, polyether antibiotics, and iridoids [1,2]. Cardiotonic, anti-tumor, anti-bronchitic, antibacterial, antimicrobial, anti-inflammatory, antimalarial, antihistamine, antiplatelet, antigenic, and antiviral actions are demonstrated by pyrano pyrimidines [3–14]. A number of condensed pyrimidine molecular systems have recently been created and tested for biological activity and fluorescence characteristics [15–19]. Many chemists are interested in 4H-pyran-annulated compounds because they have a wide range of biological and pharmacological activities as emetic, anti-HIV, anti-tumor, anti-cancer, anti-coagulant, anti-Alzheimer, anti-bacterial, anti-malaria, diuretic, spasmolytic, anti-leukemic, anti-hyperglycemic, and anti-dyslipidemic [20]. Moreover, these compounds have potential

to be employed as cognitive enhancers for the therapy of neurodegenerative disorders such as Alzheimer's, amyotrophic lateral sclerosis, AIDS-associated dementia, and Down syndrome, as well as schizophrenia and Huntington's diseases [21]. Furthermore, such functionalized 4H-pyran derivatives have been playing a greater part in synthetic methods for potential agricultural molecules, cosmetics, and pigment industries [22,23]. Between both different pyran derivatives, 4H-pyrans with cyan functionality have the potential to be used in the treatment of rheumatoid arthritis, psoriasis, and cancer, as well as laser dyes, optical brighteners, fluorescence markers, pigments, cosmetics, and potent biodegradable agrochemicals [24–29]. Some of the 4H-pyrans derivatives had high pharmacological activity. The research survey confirmed no reports on ethyl 6-amino-4-(4-chlorophenyl)-5-cyano-2- methyl-4H-pyran-3-carboxylate **(L)** (Scheme 1A) with metal ions.

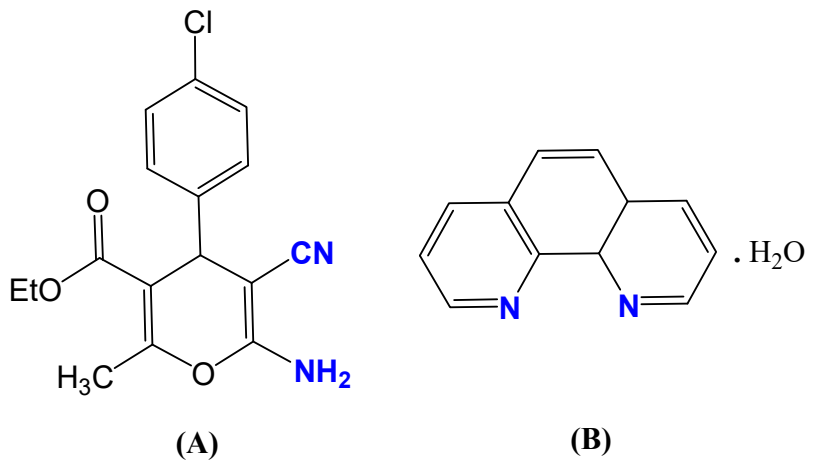

Scheme 1. (**A**) Ethyl 6-amino-4-(4-chlorophenyl)-5-cyano-2- methyl-4H-pyran-3-carboxylate (**L**) and (**B**) 1,10-phenanthroline monohydrate (**Phen**).

Phen (Scheme 1B) is a heterocyclic compound acting as a ligand, which is appealing owing to its capacity to serve as a powerful binder for double-stranded DNA and to assist in the extraction of the hydrogen atom from the sugar unit [30,31]. In the literature, there are several studies of mixed ligands metal complexes that integrate **Phen** with other ligands [32–36]. Numerous studies have also shown that the biologically relevant elements Co(II), Ni(II), Cu(II), and Zn(II) participate in a variety of structures and activities of the components of biology, thus they have also shown strong cytotoxic action when combined with a variety of ligands [37–39].

To carry out more research on mixed ligand metal complexes [40–43], the goal of the current research was to observe the interaction of some biological metals such as Cr(III), Fe(III), Co(II), Ni(II), Cu(II), and Zn(II) with **L** and **Phen** for producing some novel mixed ligand metal complexes. Elemental studies, molar conductivity, magnetic susceptibility tests, FT-IR, UV-vis, ^{1}H NMR, XRD, and thermal gravimetric analyses were used to explain the complexes' structures. Furthermore, biological activities towards some bacteria and fungi strains of the synthesized compounds were assessed.

2. Results and Discussion

2.1. Elemental Analysis and Molar Conductance

L chelated with chromium(III), iron(III), cobalt(II), nickel(II), copper(II), and zinc(II) in the existence of **Phen** to obtain complexes. The reaction system proceeds in the absence of any oxidizing agent which stabilizes the oxidation state of Co(II) in the reaction mixture in the absence of atmospheric oxygen. All complexes are stable in air, coloured, non-hygroscopic powders, and soluble in DMSO and DMF. Table 1 shows the data of CHN, melting points, and molar conductance for **L**, **Phen**, and investigated complexes. The values of molar conductance of all compounds in DMF were obtained and observed between

125.94 and 198.65 Ω cm^2 mol^{-1} for complexes, these values confirmed that the trivalent complexes were 1:3 electrolytes while, the divalent complexes were 1:2 electrolytes with chloride existing outside the complex sphere [44,45], and **L** and **Phen** ligands were found to be nonelectrolytes with values of 6.28 and 5.00, respectively.

Table 1. Elemental analysis and physico-analytical data for **L**, **Phen**, and their metal complexes.

Compounds M.Wt. (M.F.) and Cord. F.	Color Yield (%)	M.P. (°C)	Calc. (Found) (%)					Λ Ω cm^2 mol^{-1}
			C	H	N	M	Cl	
L 318.50 ($C_{16}H_{18}ClN_2O_3$)	Yellow 88.00	165	60.28 (60.01)	4.71 (4.57)	8.79 (8.68)	-	11.14 (10.99)	6.28
Phen 198.20 ($C_{12}H_{10}N_2O$)	White -	100	72.61 (72.35)	5.00 (4.89)	14.05 (13.98)	-	-	5.00
(1) 737.99 ($CrC_{28}H_{32}N_4O_{7.5}Cl_4$) $[Cr(L)(Phen)(H_2O)_2]Cl_3.2.5H_2O$	Faint Green 85.43	200	45.53 (45.22)	4.34 (4.22)	7.59 (7.37)	7.04 (6.87)	19.24 (19.01)	198.65
(2) 723.80 ($FeC_{28}H_{30}N_4O_{6.5}Cl_4$) $[Fe(L)(Phen)(H_2O)_2]Cl_3.1.5H_2O$	Dark Red 74.17	95	46.42 (46.32)	4.14 (4.05)	7.73 (7.52)	7.70 (7.46)	19.61 (19.23)	191.23
(3) 691.50 ($CoC_{28}H_{30}N_4O_{6.5}Cl_3$) $[Co(L)(Phen)(H_2O)_2]Cl_2.1.5H_2O$	Faint Green 78.33	210	48.59 (48.19)	4.34 (4.24)	8.10 (7.99)	8.52 (8.22)	15.40 (15.13)	142.35
(4) 709.20 ($NiC_{28}H_{32}N_4O_{7.5}Cl_3$) $[Ni(L)(Phen)(H_2O)_2]Cl_2.2.5H_2O$	Pale Green 78.96	280 Decomposed	47.38 (47.19)	4.51 (4.43)	7.90 (7.67)	8.28 (8.11)	15.02 (14.87)	137.58
(5) 678.00 ($CuC_{28}H_{28}N_4O_{5.5}Cl_3$) $[Cu(L)(Phen)(H_2O)_2]Cl_2.0.5H_2O$	Green 76.69	180	49.56 (49.44)	4.13 (3.99)	8.26 (8.02)	9.37 (9.13)	15.71 (15.44)	125.94
(6) 688.90 ($ZnC_{28}H_{29}N_4O_6Cl_3$) $[Zn(L)(Phen)(H_2O)_2]Cl_2.H_2O$	Buff 80.09	105	48.77 (48.34)	4.21 (4.04)	8.13 (8.01)	9.51 (9.29)	15.46 (15.25)	128.32

2.2. FT-IR Spectra

The spectra of **L**, **Phen**, and our complexes were observed (Figure S1) with details listed in Table S1. The positions of the important bands in the spectra of **L** and **Phen** were demonstrated to identify the binding sites that could be linked in coordination. The spectrum of **L** was characterized mainly by medium to very strong intensity absorption bands at 3263, 3223, and 2192 cm^{-1}. The first two bands are due to ν(N-H), while, the last band is related to ν(C≡N) [46]. In terms of a contrast of the IR data of the complexes with those of **L**, the shift of ν(N-H) to higher and/or lower frequency values (Table S1) in the spectra of the complexes could imply an increase in N-H bond strength throughout chelation [46,47]. The change in intensity of C≡N in all complexes from very strong to medium proves that the **L** molecule binds with metal ions via the nitrogen atom of the cyano group (Scheme 2) [47]. Furthermore, the shift of ν(C≡N) in some complexes from 2192 to around 2228 confirmed the chelation from the lone pair of electrons on the N atom in the cyano group with metal ions [48,49]. The potential that coordination to metal ions reduces the electron density on the nitrogen atom means that it attracts single bond electrons, resulting in a stronger N-H bond and then a higher frequency bond. While the shift of ν(C≡N) intensity to a lower value confirms the presence of a CN group in the interaction with L forming five membered rings around the metal ion. The detected peak at 1586 cm^{-1} in **Phen**, which may be assigned to ν(C=N), moved to lower frequencies in the metal complexes, showing the role of pyridine ring nitrogen in complex development [31,32,50]. The existence of strong and broad bands at 3321–3406 cm^{-1} represents ν(O–H) stretching vibrations, proving that all complexes contain coordinated and/or hydrated water molecules [31,32,51]. The complexes' spectra involve some new

bands with different intensities for ν(M-O) and ν(M-N), which were discovered at 719 and 505,722 and 516,721 and 506,725 and 507,719 and 629, and 732 and 507 cm^{-1} for complexes **(1)**, **(2)**, **(3)**, **(4)**, **(5)**, and **(6)**, respectively.

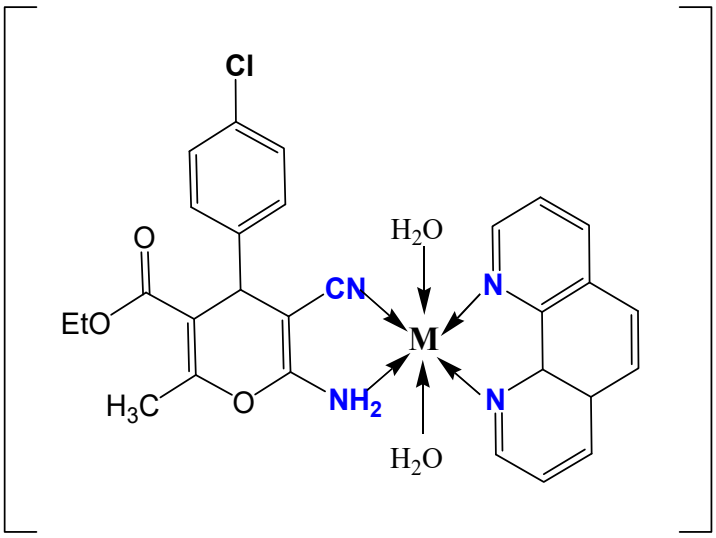

No.	M	n	m
(1)	Cr	3	2.5
(2)	Fe	3	1.5
(3)	Co	2	1.5
(4)	Ni	2	2.5
(5)	Cu	2	0.5
(6)	Zn	2	1.0

Scheme 2. Proposed structure for metal complexes.

2.3. UV-vis. Spectra and Magnetic Moment

In DMSO, the electronic absorption spectra of **L**, **Phen**, and their complexes were observed between 200 and 800 nm (Figure S2). The outcomes assigned that **L** showed two bands at 284 and 343 nm, which may be related to π-π* and n-π* transitions, respectively (Table 2). Furthermore, **Phen** bands were observed at 300 and 340 nm, which referred to π-π* and n-π*transitions [31,52]. The complexes **(1)**, **(2)**, **(3)**, **(4)**, and **(5)** are paramagnetic because of the presence of an unpaired electron and their d-d transition spectra obtained at 19,047 cm^{-1} for complex **(1)** with 10Dq value at 227.8 kJ mol^{-1} with CFSE at −273.36, which is assigned as $^4A_{2g}(F) \rightarrow {}^4T_{2g}(F)$, at 13,850 cm^{-1} for complex **(2)** with 10Dq at 165.6 kJ mol^{-1}, which is referred to as $^6A_{1g} \rightarrow {}^4T_{1g}(G)$, at 16,129 for complex **(3)** with 10Dq at 192.9 kJ mol^{-1} and CFSE at −154.3 + 2p, which refer to $^4T_{1g}(F) \rightarrow {}^4A_{2g}(F)$, at 15,384 cm^{-1} for complex **(4)** with 10Dq at 184.0 kJ mol^{-1} and CFSE at 220.8 + 3p, which is assigned as $^3A_{2g}(F) \rightarrow {}^3T_{2g}$, and at 16,260 cm^{-1} for complex **(5)** with 10Dq at 194.5 kJ mol^{-1} and CFSE at 116.7+4p, which is assigned as $^2E_g \rightarrow {}^2T_{2g}$ [53–57]. The magnetic susceptibilities (μ_{eff}) of the complexes were evaluated and found at 3.32, 5.90, 4.22, 3.05, and 1.76 B.M. for complexes **(1)**, **(2)**, **(3)**, **(4)**, and **(5)**, respectively. The molar absorptivity (ε) values of the synthesized complexes were obtained by using Equation (1):

$$A = \varepsilon cl \quad (1)$$

where A = absorbance, l = cell length of 1 cm, and c = 1.0×10^{-3} M.

Table 2. UV-vis. Spectra for **L**, **Phen**, and their metal complexes.

Compound	λ_{max} (nm)	ν (cm^{-1})	Peak Assignment	ε ($M^{-1}cm^{-1}$)	10Dq		CFSE	μ_{eff} (B.M)
					cm^{-1}	kJ/mol		
L	284	35,211	π→π *	12	-	-	-	-
	343	29,154	n→π *	104				
Phen	275	36,364	π→π *	27	-	-	-	-
	355	28,169	n→π *	235				
(1)	255, 305	39,215, 32,786	π→π *	42, 30	19,047	227.8	−273.36	3.32
	354	28,248	n→π *	15				
	475, 490	21,052, 20,408	LMCT	358, 270				
	525	19,047	d-d transition	125				
(2)	250, 280	40,000, 35,714	π→π *	45, 100	13,850	165.6	0.00	5.90
	345	28,985	n→π *	55				
	485, 570	20,618, 17,543	LMCT	600, 1341				
	722	13,850	d-d transition	24				
(3)	290	34,482	π→π*	90	16,129	192.9	−154.3 + 2p	4.22
	350	28,571	n→π*	53				
	465, 490	21,505, 20,408	LMCT	47, 285				
	620	16,129	d-d transition	478				
(4)	250, 290	40,000, 34,482	π→π *	38, 40	15,384	184.0	220.8 + 3p	3.05
	320	31,250	n→π *	20				
	460, 490	21,739, 20,408	LMCT	442, 457				
	650	15,384	d-d transition	43				
(5)	255	39,215	π→π *	34	16,260	194.5	116.7 + 4p	1.76
	300, 330	33,333, 30,303	n→π *	25, 18				
	460, 490	21,739, 20,408	LMCT	442, 445				
	615	16,260	d-d transition	56				
(6)	255	39,215	π→π *	53	-	-	-	-
	310, 350	32,258, 28,571	n→π *	60, 30				
	420, 470, 490	23,809, 21,276, 20,408	LMCT	66, 388, 299				

2.4. ^{1}H NMR and ^{13}C NMR Spectra

The proposed structures of **L, Phen** and Zn(II) complex were characterized by ^{1}H, ^{13}C NMR spectroscopy in DMSO-d_6 as a solvent (Figure 1). ^{1}H NMR of **L**: δ (1.03) (t, J = 3.09, 3H, –CH_2CH_3), 2.30 (s, J = 6.9, 3H, –CH_3), 3.96 (q, J = 11.88, 2H, –CH_2CH_3), 4.31 (s, J = 12.93, 1H, –H-pyran) 6.95 (s, J = 28.95,2H, –NH_2), 7.15–7.35 (d, J = 0.6, 2H, -H-aromatic), 3.82 (s, J = 11.46, 2H, H_2O). ^{13}C NMR (DMSO-d_6, 100 MHz): δ_C = 18.50, 24.26, 57.86, 61.96, 108.4, 116.2, 123.5, 128.6, 130.6, 131.6, 142.7, 157.3, 162.3 and 165.5. Furthermore, ^{1}H NMR spectrum of Zn(II) complex was obtained: δ(1.01–3.95) (t, J = 8.82, 3H, –CH_2CH_3), 2.29 (s, J = 6.87, 3H, –CH_3), 4.29 (s, J = 12.87, 1H, –H-pyran) 6.97 (s, J =20.91, 2H, –NH_2), 7.29–8.00 (d, J = 2.13, 2H, -H-aromatic). In Zn(II) complex spectrum, **L** peaks possess some shifts from the binding of **L** to Zn(II). Furthermore, H_2O has a new peak at δ 3.82 [58].

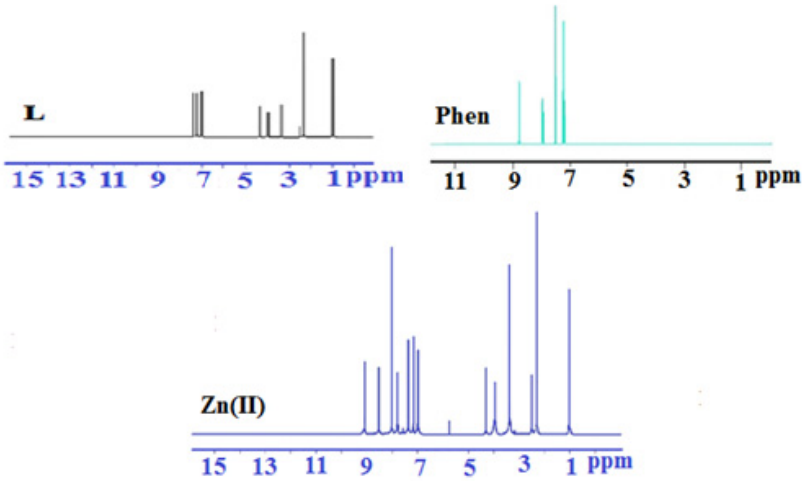

Figure 1. ^{1}H NMR spectra, for **L**, **Phen**, and Zn(II) complex.

2.5. Thermal Analyses

Thermal analyses were carried out with the aim to investigate the kind of H_2O in the investigated compounds. In the proposed structure for our complexes, the type of adsorbed or lattice H_2O molecules that are found outside the inner coordination sphere of the central metal ion will move away from the structure at below 120 °C. However, the second type of H_2O molecules were found inside the complex sphere and formed coordinated bonds with metal ions; this type of water moves away from the structure at above 120 °C. The TG curve (Figure S3) of **L** with melting point (M.P.) at 165 °C initiated at 137 °C and completed at 761 °C (Table S2), with two steps. The 1st stage occurs at T_{max} 239 °C with a drop in mass of 62.95% (calc. 62.63%), relating to the removal of CH_4+$2C_2H_2$+2CO+C_3H_4+$0.5Cl_2$; this step is characterized by activation energy (E_a) of 185.56 kJ mol^{-1} and the reaction order is 0.981. Furthermore, it was confirmed with DTA endothermic peaks at −24.85 and −8.40 µV. The 2nd step at T_{max} of 318 and 520 °C with a drop in mass of 36.94% (calc. 37.37%), refers to the loss of C_4H_2+$0.5N_2$+HCN, and is confirmed by exothermic DTA at 3.39 µV. According to the literature survey, the thermogram of **Phen** with M.P. at 100 °C indicates two successive stages of degradation [54]. The TG diagram of complex **(1)** (M.P. 200 °C) initiated at 40 °C and completed at 889 °C, with three steps. The 1st one was found at T_{max} 85 °C with mass loss of 6.00% (calc. 6.09%) and was assigned to the removal of $2.5H_2O$ with DTA endothermic peak at −0.75 and −2.24 µV. The 2nd stage at a maximum of 255 °C with a drop in mass of 29.11% (calc. 29.27%) was assigned to the removal of $6C_2H_2$+2NO and supported by E_a = 35.11 kJ mol^{-1}. The last step at T_{max} 477 and 770 °C with 57.41% overall weight loss (calc. 57.59%) was assigned to the removal of $7C_2H_2$+NO+CO_2+$2Cl_2$+HCN and supported by endothermic DTA peak at −1.19, −2.29, and −0.67 µV, leaving Cr as residue. Complex **(2)** with M.P. at 95 °C follows three degradation phases: The 1st step at 87 °C, with a weight loss of 3.70% (calc. 3.74%) was related to removal of 1.5 H_2O. The 2nd step at T_{max} 226 °C with a drop in mass of 44.88% (calc. 44.55%) was assigned to the loss of $6C_2H_2$+2NO+$1.5Cl_2$, and confirmed with endothermic DTA peak at 3.56 µV and E_a at 27.96 kJ mol^{-1}. The 3rd step at T_{max} 383 and 511 °C with mass loss of 45.15% (calc. 44.01%) associated with liberation of $7C_2H_2$+HCN+NO+CO_2+$0.5Cl_2$, with one endothermic peak at 15.40 µV, leaving iron as a residue. Complex **(3)** with M.P. at 210 °C follows four degradation phases. The 1st step found at 79 °C, with a drop in mass of 3.88% (calc. 3.90%), involved the removal of lattice water with DTA endothermic peak at −8.63 µV. The 2nd decomposition step at T_{max} 198 °C with 32.76% overall weight loss (calc. 31.24%) liberated $6C_2H_2$+N_2+O_2, and was confirmed with two DTA endothermic peaks at −6.73 and −3.78 µV with E_a at 44.16 kJ mol^{-1}. The 3rd step at T_{max} 388 °C with 10.37% overall weight loss (calc. 10.12%) was assigned to the removal of Cl_2. The 4th step at T_{max} 640 °C with a drop in mass of 43.41% (calc. 43.74%) liberated $7C_2H_2$+2CO+HCl+N_2, with one endothermic peak at −1.32 µV,

leaving CoO as residue. Complex **(4)** (M.P. 280 °C) follows three degradation phases. The 1st step obtained at 68 °C, with a drop in mass of 6.31% (calc. 6.34%) related to the release of $2.5H_2O$ with two DTA endothermic peaks at −5.34 and −1.68 µV. The 2nd step at T_{max} 183 °C with a drop in mass of 39.68% (calc. 40.46%) liberated $6C_2H_2$+Cl_2+O_2+N_2, and was confirmed with a DTA exothermic peak at −2.20 µV and E_a at 30.38 kJ mol^{-1}. The 3rd step at T_{max} 405 °C with a drop in mass of 47.19% (calc. 46.97%) was assigned to removal of $7C_2H_2$+HCN+NO+CO_2+$0.5Cl_2$, with one endothermic peak at −0.88 µV, leaving Ni as a residue. Complex **(5)** with M.P. at 180 °C follows three decomposition phases: the 1st step at 58 °C, with a drop in mass of 1.34% (calc. 1.33%) corresponding to the release of 0.5 H_2O. The 2nd step at T_{max} 182 and 358 °C with a drop in mass of 41.76% (calc. 42.33%) was assigned to the removal of $6C_2H_2$+2NO+Cl_2, and was confirmed with DTA endothermic peak at −4.24 µV and E_a at 48.70 kJ mol^{-1}. The 3rd step at 639 and 844 °C maxima with 47.16% overall weight loss (calc. 46.98%) liberated $7C_2H_2$+CO+CO_2+N_2+HCl, with one endothermic peak at −0.99 µV, leaving Cu as a final product. Finally, complex **(6)** (M.P. 105 °C) follows four degradation phases. The 1st step at 87 °C, with 2.66% overall weight loss (calc. 2.61%) related to the release of H_2O, and was validated with DTA endothermic peak at −10.23 µV. The 2nd stage at 164, 268, and 491 °C maxima with 57.58% overall weight loss (calc. 57.99%) was assigned to removal of $8C_2H_2$+HCl+Cl_2+2CO+N_2, and was proven by DTA endothermic peak at −7.47 µV and DTA exothermic peak at 3.20 µV with E_a at 42.50 kJ mol^{-1}. The 3rd step at T_{max} 607 °C with 18.00% overall weight loss (calc. 17.99%) liberated $3C_2H_2$+CO+H_2O, with one exothermic peak at 24.68 µV. The last step at T_{max} 844 °C with a drop in mass of 12.39% (calc. 11.90%) was assigned to the removal of C_2H_2+CO+N_2, with one endothermic peak at −2.90 µV, leaving Zn metal as residue.

2.6. The Kinetic Data

The activated thermodynamic parameters, activation energy (E_a), enthalpy (ΔH*), entropy (ΔS*), and Gibbs free energy (ΔG*) were computed using Coats–Redfern (CR) and Horowitz–Metzger (HM) methods (Figure S4) [59,60].

$$\ln X = \ln\left[\frac{1-(1-\propto)^{1-n}}{T^2(1-n)}\right] = \ln\left(\frac{AR}{\beta E}\right) - \frac{E_a}{RT} \text{ for } n \neq 1 \quad (2)$$

$$\ln X = \ln\left[\frac{-\ln(1-\propto)}{T^2}\right] = \ln\left(\frac{AR}{\beta E}\right) - \frac{E_a}{RT} \text{ for } n = 1 \quad (3)$$

$$\ln[-\ln(1-\propto)] = \frac{E_a\theta}{RT_s^2} \text{ for } n = 1 \quad (4)$$

$$\ln\left[\frac{1-(1-\propto)^{1-n}}{1-n}\right] = \ln\left(\frac{A}{\beta}\frac{RT_s^2}{E}\right) - \frac{E_a}{RT_s} + \frac{E_a\,\theta}{RT_s^2} \text{ for } n \neq 1 \quad (5)$$

$$\Delta H^* = E_a - RT \quad (6)$$

$$\Delta S^* = R\ \ln\frac{hA}{K_B T} \quad (7)$$

$$\Delta G^* = \Delta H^* - T\Delta S^* \quad (8)$$

For Arrhenius, the correlation coefficient plots of thermal decomposition phases were observed in the 0.758–0.998 zone, showing a good fit with the linear function. E_a of degradation were observed between 8.53 and 146.78 kJ mol^{-1} (Table 3) [45,61]. The negative values of ΔS* of the degradation steps for metal complexes imply that the activated fragments are more organized than the undecayed complexes or that the decayed activities are slow. The positive sign of ΔH* assigned to the degradation steps demonstrates that the steps of breakdown are endothermic. Furthermore, positive ΔG* values suggest that the

free energy of the end residue is greater than that of the starting molecules, and all break phases are nonspontaneous processes [45,62].

Table 3. Thermal behavior and kinetic parameters for **L**, **Phen**, and metal complexes.

Compounds	Decomposition Range (K)	T_s (K)	Method	Parameter					R [a]	SD [b]
				E_a (kJ/mol)	A (s^{-1})	ΔS* (kJ/mol·K)	ΔH* (kJ/mol)	ΔG* (kJ/mol)		
L	436–540	512	CR	185.56	5.08×10^{18}	0.0746	181.30	143.07	0.981	0.034
			HM	157.18	7.81×10^{15}	0.0208	152.92	142.27	0.970	0.036
Phen	394–572	551	CR	117.83	2.03×10^{9}	−0.071	113.250	152.84	0.996	0.120
			HM	146.78	7.97×10^{11}	−0.022	142.210	154.42	0.998	0.076
(1)	313–683	529	CR	35.11	5.72×10^{2}	−0.2309	30.71	152.87	0.948	0.105
			HM	47.13	2.11×10^{10}	−0.0860	42.73	88.24	0.951	0.097
(2)	310–690	656	CR	27.96	17.00	−0.2619	22.51	194.32	0.909	0.102
			HM	53.91	2.94×10^{3}	−0.2190	48.46	192.17	0.883	0.198
(3)	292–617	198	CR	44.16	6.03×10^{4}	−0.1840	42.51	78.94	0.976	0.043
			HM	8.53	7.18×10^{10}	−0.0336	6.89	13.56	0.968	0.057
(4)	313–646	457	CR	30.38	1.89×10^{2}	−0.2389	26.59	135.76	0.955	0.051
			HM	40.49	9.87×10^{3}	−0.2060	36.69	130.84	0.948	0.094
(5)	292–650	455	CR	48.70	2.33×10^{4}	−0.1988	44.91	135.39	0.842	0.265
			HM	38.55	5.95×10^{3}	−0.2101	34.77	130.40	0.758	0.407
(6)	332–602	437	CR	42.50	4.88×10^{3}	−0.2115	38.86	131.29	0.947	0.036
			HM	35.10	3.45×10^{3}	−0.2143	31.47	125.15	0.979	0.092

a = correlation coefficients of the Arrhenius plots; b = standard deviation.

2.7. XRD

The crystallinity and the diffraction patterns of **L**, **Phen**, and their metal complexes were obtained over the assessing range of 2θ = 0–80° (Figure 2). According to the strong sharp peaks, the prepared complexes have high crystallinity. Table 4 includes details of the diffractograms and associated data, such as the relative intensity, the inter-planar spacing (d-values), and the 2θ values (for each peak). Significant peaks with relative intensity greater than 10% were found in the XRD pattern of our compounds. The last outcome proved that the ligand and the complexes are crystalline in nature. The XRD pattern of **L** found at 100% intensity was determined at 2θ = 17.99°. The data recorded in the literature review for **Phen** showed the crystallinity in the range 2θ = 0–56° [32]. The main peaks for **Phen** were determined at 2θ = 19.87°. Sharp peaks represent strong crystallinity in the synthesized complexes [45,63]. The diffraction peaks at maximum intensity (100%) for complex **(1)** were found at 2θ = 21.90°. The XRD peaks of **(2)** were recognized at 2θ = 22.33°; for **(3)**, at 2θ = 28.54°; for **(4)**, at 2θ = 24.34°; for **(5)**, at 2θ = 27.66°; and for **(6)**, at 2θ = 31.66°. The Debye–Scherer Equation (8) was used to determine the crystallite sizes of tested compounds.

$$Cs = \frac{K\lambda}{\beta cos\theta} \quad (9)$$

where, k is the Scherer constant = 0.9, λ is the X-ray beam wavelength = 0.15405 nm, β is the full width at half maximum (FWHM) of the diffracted peak in radians, and θ is the diffraction angle (radians) [64,65].

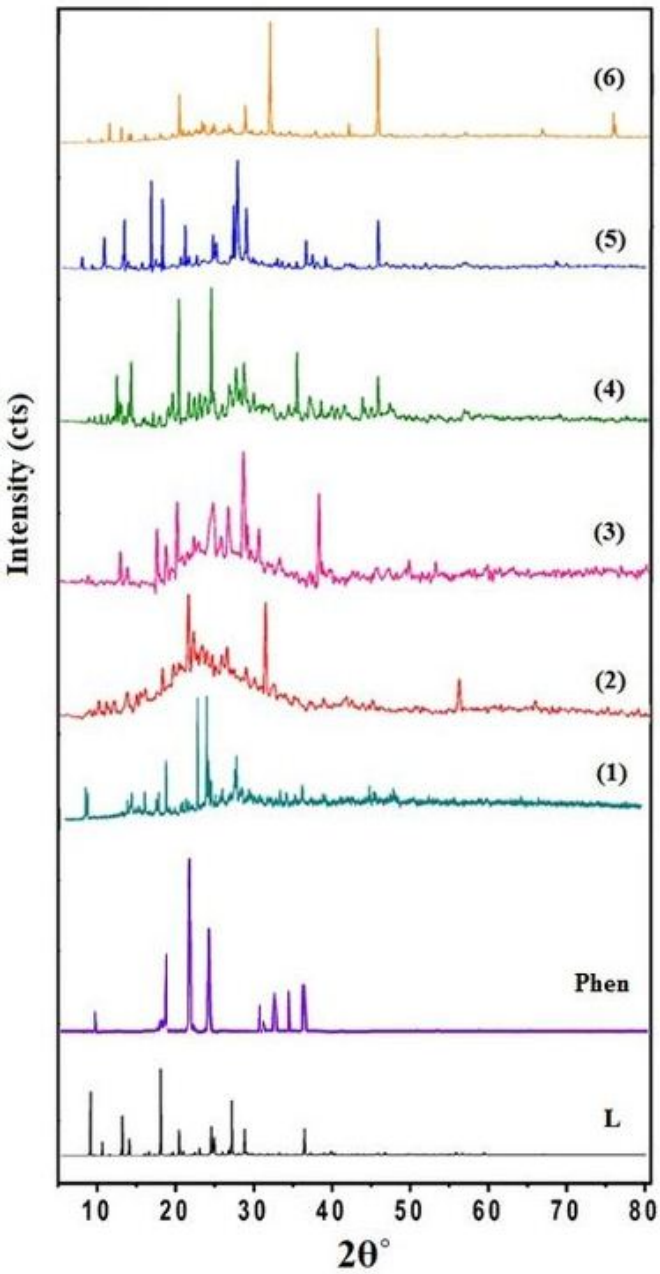

Figure 2. XRD spectra of **L**, **Phen**, and their metal complexes.

Table 4. The average crystallite size of **L**, **Phen**, and their metal complexes estimated from XRD patterns.

Compounds	2θ (°)	d (A°)	FWHM	C_s (nm)	$D \times 10^{-4}$ (nm^{-2})	$\varepsilon \times 10^{-2}$ (rad)
L	17.99	4.95	0.1771	45.41	4.84	27.97
Phen	19.87	4.47	0.2170	38.93	7.24	30.97
(1)	21.90	4.07	0.0984	82.22	1.47	12.71
(2)	22.33	4.00	0.2558	31.65	9.98	32.40
(3)	28.54	3.14	0.1574	52.07	3.68	15.47
(4)	24.34	3.67	0.1378	58.97	2.87	15.97
(5)	27.66	3.24	0.2168	37.78	7.00	22.02
(6)	31.66	2.84	0.1771	46.62	4.60	15.62

C_s values of the investigated compounds were obtained in the range of 31.65 to 82.22 nm (nano-size structures) as listed in Table 4. Dislocation density value (D) was in the range of 1.47×10^{-4} to 9.98×10^{-4} nm^{-2}, by which D and micro strain (ε) can be determined using Equations (10) and (11) [66].

$$D = \frac{1}{C_s^2} \tag{10}$$

$$E = \frac{\beta}{4tan\theta} \tag{11}$$

2.8. Antimicrobial Efficiency

The antimicrobial effectiveness of **L**, **Phen**, and their metal complexes against two gram-positive bacteria (*Staphylococcus aureus* and *Bacillus subtilis*), two gram-negative bacteria (*Escherichia coli* and *Pseudomonas aeruginosa*) and two fungi (*Candida albicans* and *Aspergillus flavus*) using the disk diffusion technique. MIC and AI values are illustrated in Table 5 and in Figures 3 and S5, respectively. For metal salts, no growth inhibition was obtained, indicating that they are not subjected to the observed antimicrobial activity obtained from the studied metal complexes [67–70]. Complex **(1)** was significant against *S. aureus*, *B. subtilis*, *P. aeruginosa*, *C. albicans*, and *A. flavus* and showed non-significant activity towards *E. coli*. For complex **(2),** no detectable effects against all tested fungi and bacteria except *B. subtilis* were non-significant. Complex **(3)** explicated high significance towards all tested bacteria except *E. coli* and significance against *E. coli* and two fungi. Complex **(4)** indicated non-significant effect towards all tested microorganisms except *C. albicans*, which is significant. Complex **(5)** is non-significant towards all tested microorganisms and non-detectable towards *C. albicans*. Complex **(6)** indicated non-significant activity towards all microorganisms but significant towards *C. albicans*. The data reported in a comparative study of two ligands and their metal complexes showed that the complexes exhibited higher antimicrobial activity than the ligands and standard references. The increase in activity of metal chelates can be explained based on the overtone concept and chelation theory. Complex **(3)** is the most active of the two ligands, other complexes, and standard references towards tested bacterial and fungi. The higher antimicrobial activity of Co(II) complex might be attributed to the higher reactivity of Co(II), replacing the metals of metalloenzyme, especially respiratory enzymes and all oxidoreductase enzymes causing cellular growth arrest, as well as, the displacement of metals from metalloenzymes, causing enzyme denaturation with predictable loss to enzyme activity [71]. The second explanation for the Co(II) complex's greater antimicrobial activity may be related to the production of DNA-metals adducts that damage, mutate, and ultimately prevent DNA replication as well as transcription and translation [72]. Of note, the lipid membrane that surrounds the cell, which permits lipid-soluble chemicals to penetrate and is an essential component of antimicrobial action, can be used to characterize increasingly more beneficial complexes. This indicates that chelation might promote metal complex diffusion across the lipid section of the cell membrane and into the action region [73–75].

Table 5. Antimicrobial activities of **L**, **Phen**, and metal complexes.

Compounds	G(+ve) and G(−ve) Bacterial Strains											
	S. aureus			*B. subtilis*			*E. coli*			*P. aeruginosa*		
	D.iz [a] (mm)	AI [b] (%)	MIC [c] (µg/mL)	D.iz (mm)	AI (%)	MIC (µg/mL)	D.iz (mm)	AI (%)	MIC (µg/mL)	D.iz (mm)	AI (%)	MIC (µg/mL)
L	9 ± 0.22	37.5	0.050	13 ± 0.05	56.5	0.100	8 ± 0.01	32.0	0.050	10 ± 0.33	43.5	0.075
Phen	$7^{NS} \pm 0.55$	29.2	0.075	$9^{NS} \pm 0.11$	39.1	0.075	ND	—	—	$4^{NS} \pm 0.11$	17.4	0.050
(1)	$11^{+1} \pm 0.08$	45.8	0.100	$15^{+1} \pm 0.88$	65.2	0.100	$10^{NS} \pm 0.11$	40.0	0.075	$13^{+1} \pm 0.05$	56.5	0.100
(2)	ND	—	—	$3^{NS} \pm 0.60$	13.0	0.025	ND	—	—	ND	—	—
(3)	$14^{+2} \pm 0.06$	58.3	0.100	$17^{+2} \pm 0.01$	73.9	0.100	$11^{+1} \pm 0.09$	44.0	0.100	$16^{+2} \pm 0.60$	69.6	0.100
(4)	$9^{NS} \pm 0.44$	37.5	0.075	$11^{NS} \pm 0.03$	47.8	0.075	$8^{NS} \pm 0.77$	32.0	0.025	$9^{NS} \pm 0.09$	39.1	0.050
(5)	$5^{NS} \pm 0.33$	20.8	0.025	$8^{NS} \pm 0.22$	34.8	0.025	$6^{NS} \pm 0.22$	24.0	0.050	$9^{NS} \pm 0.33$	39.1	0.075
(6)	$4^{NS} \pm 0.07$	16.7	0.050	$6^{NS} \pm 0.09$	26.1	0.050	$3^{NS} \pm 0.01$	12.0	0.025	$5^{NS} \pm 0.77$	21.7	0.025
Standards Ampicillin	24 ± 0.02	100	0.100	23 ± 0.07	100	0.100	23 ± 0.22	100	0.100	23 ± 0.22	100	0.100
Standards Clotrimazole	ND	—	—	ND	—	—	ND	—	—	ND	—	—

Compounds	Fungal Strains					
	C. albicans			*A. flavus*		
	D.iz (mm)	AI (%)	MIC (µg/mL)	D.iz (mm)	AI (%)	MIC (µg/mL)
L	12 ± 0.14	44.4	0.100	14 ± 0.16	56.0	0.100
Phen	$10^{NS} \pm 0.11$	37.0	0.075	$12^{NS} \pm 0.11$	48.0	0.050
(1)	$16^{+1} \pm 0.22$	59.2	0.100	$18^{+1} \pm 0.09$	72.0	0.100
(2)	ND	—	—	ND	—	—
(3)	$15^{+1} \pm 0.55$	55.5	0.100	$16^{+1} \pm 0.8$	64.0	0.050
(4)	$7^{+1} \pm 0.09$	25.9	0.075	$9^{NS} \pm 0.02$	36.0	0.025
(5)	ND	—	—	$7^{NS} \pm 0.11$	28.0	0.075
(6)	$5^{+1} \pm 0.22$	18.5	0.050	$9^{NS} \pm 0.70$	36.0	0.050
Standards Ampicillin	ND	—	—	—	—	—
Standards Clotrimazole	27 ± 0.11	100	0.100	25 ± 0.02	100	0.100

Statistical significance: P^{NS}, P not significant, $p > 0.05$; P^{+1}, P significant, $p < 0.05$; P^{+2}, P highly significant, $p < 0.01$; P^{+3}, P very highly significant, $p < 0.001$; student's *t*-test (paired). [a] D.iz: inhibition zone diameter (mm); [b] AI: activity index (%); [c] MIC: minimum inhibitory concentration (µg/mL); ND: not detectable.

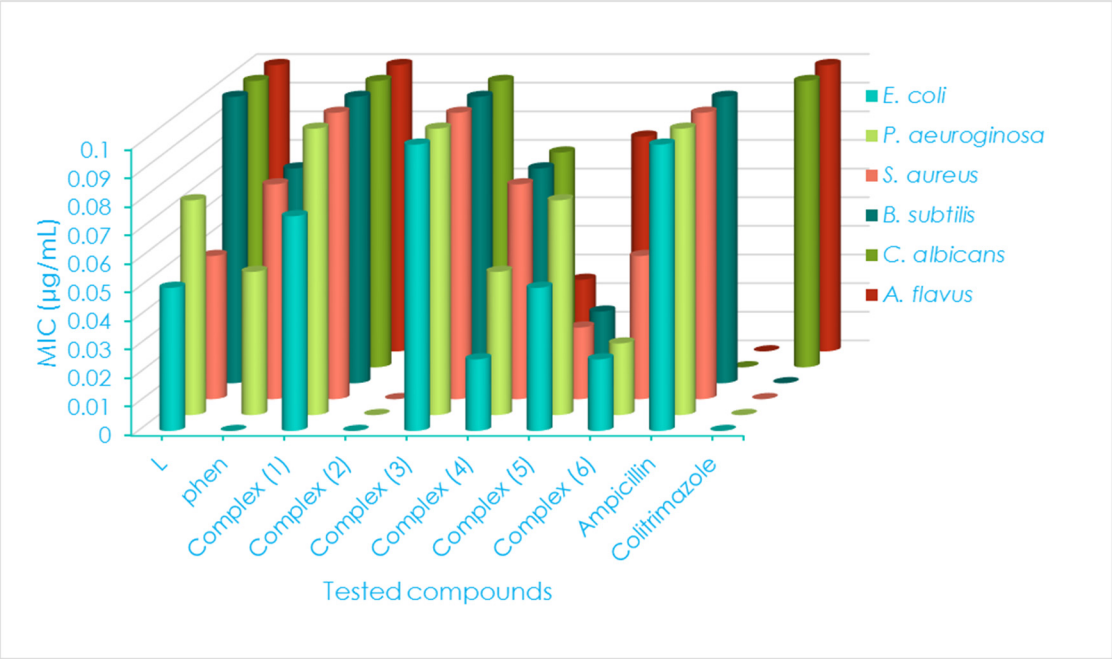

Figure 3. MIC of the microorganisms for **L**, **Phen**, and metal complexes.

3. Experimental

3.1. Materials

The chemicals and solvents employed in this study for synthesis of **L** and its metal complexes, ethyl acetoacetate, pyridine, cinnamonitrile derivative, **Phen**, ethanol $AgNO_3$, $CrCl_3.6H_2O$, $FeCl_3$, $CoCl_2.6H_2O$, $NiCl_2.6H_2O$, $CuCl_2$, and $ZnCl_2$ were of analytical grade (Merck, Sigma Aldrich, and BDH) and utilized unpurified.

3.2. Physical Techniques

Fourier-transform infrared spectra were located between 4000 and 400 cm^{-1} using an FT-IR 460 Plus spectrophotometer. A Perkin Elmer-2400 elemental analyzer was employed to carry out CHN analyses. Metal ion contents of investigated complexes were observed complexometrically, gravimetrically, and by atomic absorption [51,56]. To this aim, a PYE-UNICAM SP 1900 spectrometer equipped with the appropriate lamp was employed. The chloride content was determined using Mohr's technique [76]. Molar conductivity analysis was performed in DMF solution (10^{-3} M) by CONSORT K410. Melting points were measured using a Buchi apparatus. A Shimadzu UV3101PC was utilized to obtain the electronic absorption spectra in DMSO. A Varian Mercury VX300 NMR spectrometer was used to obtain ^{1}H NMR spectra by using DMSO-d_6. The thermal analyses (TG, DTG and DTA) were performed using a Shimadzu TG-60H thermal analyzer under nitrogen atmosphere with a flow rate of 30 mL/min and heating rate of 10 °C/min within the range of 25–1000 °C using platinum crucibles. A Sherwood scientific magnetic balance was employed to perform the magnetic susceptibilities using a modified Gouy methodology and diamagnetic corrections were computed using Pascal's constants [77]. X-ray powder diffraction investigations (XRD) were obtained by utilizing a diffractometer (Panalytical XPERT PRO MPD). Cu-Kα radiation (λ = 1.5418 Å) was performed at 40 kV to 40 mA. Antimicrobial activity of the investigated compounds was carried out at the Laboratory of Phytopathology, SAFE, University of Basilicata, Potenza, Italy.

3.3. Synthesis of *L*

L was prepared according to the published literature [78,79]. A mixture of 4-chlorobenzylidenemalononitrile (0.01 mol, 1.8861 g) and ethyl acetoacetate (0.01 mol, 1.27 mL) was mixed in 20 mL ethanol with a few drops of pyridine. The mixture was refluxed at 60 degrees for 6 h. The mixture was cooled overnight and a yellow precipitate developed which was filtered and dried under vacuum over $CaCl_2$.

3.4. Syntheses of Metal Complexes

The faint green solid complex [Cr(**L**)(**Phen**)$(H_2O)_2$]Cl_3.2.5H_2O **(1),** brown red complex [Fe(**L**)(**Phen**)$(H_2O)_2$]Cl_3.1.5H_2O **(2)**, dark green complex [Co(**L**)(**Phen**)$(H_2O)_2$]Cl_2.1.5H_2O **(3)**, dark brown complex [Ni(**L**)(**Phen**)$(H_2O)_2$]Cl_2.2.5H_2O **(4)**, brown complex [Cu(**L**)(**Phen**)$(H_2O)_2$]Cl_2.0.5H_2O **(5)**, and brown complex [Zn(**L**)(**Phen**)$(H_2O)_2$]Cl_2.H_2O **(6)** were synthesized by adding 0.5 mmol of chloride salts of the metal ions used in 20 mL ethanol to form a mixture of 50 mL of 0.5 mmol of **L** and **Phen**. The reactants were stirred with reflux for 16 h at ≈85 °C. The obtained colored solids were filtered, cleaned with C_2H_5OH, and dried under vacuum over $CaCl_2$.

3.5. Antimicrobial and Minimal Inhibitory Concentrations

Antibacterial activity of **L**, **Phen**, and their complexes were examined by a modified Beecher and Wong methodology [80] against two gram-positive bacteria (*S. aureus* and *B. subtilis*), two gram-negative bacteria (*E. coli* and *P. aeruginosa*) and two fungi (*C. albicans* and *A. flavus*). The strains of microorganisms used were obtained from the microbiological collection of the School of Agricultural, Forestry, Food and Environmental Sciences (SAFE), University of Basilicata, Potenza, Italy, and were recultured and conserved as explained by Elshafie et al. [81,82]. The Müller–Hinton agar medium (MHA) for antibacterial activity (0.2 g/L beef extract, 17.5 g/L acid hydro lysate of casein, 1.5 g/L starch and 17 g/L agar) was prepared. After autoclaving, it was cooled to 47 °C and then poured onto sterilized Petri dishes (plate of 12 cm diameter). Plates were infected with tested bacteria by dipping a sterile swab into the inoculum and then streaking the swab all over the surface of the medium twice, rotating the plates by 60 °C after every attempt. After this, swabs were discarded into an appropriate container. Furthermore, the inoculum was left to dry for a few minutes at room temperature. Whatman No. 1 filter papers with a diameter of 6 mm were put in a Petri dish and sterilized in an autoclave for 40 min. After this, disks

impregnated with appropriated antimicrobial were carefully lowered down onto the agar surface with a pair of sterile forceps to achieve total connection with the agar surface. The plates had been left at 37 degrees Celsius in an incubator. After being left overnight, the diameter of each inhibitory zone (which involves the diameter of the disk) was obtained and documented in mm using a ruler. The Czapex–Dox agar medium (30 g/L sucrose, 3 g/L sodium nitrate, 1 g/L dipotassium hydrogen phosphate, 0.05% potassium chloride, 0.001% ferrous sulphate, and 20 g/L agar) was prepared. After autoclaving, it was left to cool to 47 °C and then seeded with tested fungal strain. After this, media was poured into sterile Petri dishes and left to solidify. After solidification, 5 mm diameter holes were punched with a sterile cork-borer. Ligands and their complexes were dissolved in DMSO (1×10^{-3} M), and then inoculated in Petri dishes (only 0.1 mL). After this, plates were incubated at 30 °C for 7 days. The diameter of the inhibitory zone was used to calculate activity (in mm). The index percent activity of the compounds was calculated (Equation (12)):

$$Activity\ Index\ (AI) = \frac{Inhibition\ zone\ by\ test\ compound\ diameter}{Inhibition\ zone\ by\ standard\ diameter} \times 100 \quad (12)$$

MIC determined for **L**, **Phen**, and metal complexes towards the above-mentioned tested bacterial and fungal strains were obtained using the standard broth microdilution method in LB broth [83]. Metal compounds were investigated at concentrations ranging from 0.025 to 0.100 μg/mL, using DMSO solvent as standard.

4. Conclusions

This investigation was accepted for the synthesis previously prepared new mixed ligand complexes of Cr and Fe trivalent and Co, Ni, Cu, and Zn divalent ions with **L** and **Phen**. Spectroscopic and physicochemical techniques were utilized to characterize the new mixed metal complexes. In all these complexes, both **L** and **Phen** behaved as bidentate ligands via the nitrogen of the amino group, nitrogen of the cyano group, and two nitrogen atoms of the pyridine group, respectively. Molar conductance proved that all prepared complexes are electrolyte in nature with different Cl^- ions found out the outer sphere of the complexes. The antimicrobial activity of two ligands and all generated complexes has been examined towards Gram-positive and Gram-negative bacteria and two fungi strains. In addition, Co(II) complex has a significant efficiency toward bacteria, and Cr(III) complex is highly significant towards fungal strains compared to other compounds.

Supplementary Materials: The following supporting information can be downloaded at: https://www.mdpi.com/article/10.3390/inorganics11050220/s1. Figure S1: FT-IR spectra for **L**, **Phen** and their complexes; Figure S2: UV-vis. spectra for **L**, **Phen** and their complexes; Figure S3: TG, DTG and DTA diagrams for L, **Phen** and their complexes; Figure S4: Kinetic parameters diagrams of **L**, **Phen** and their metal complexes; Figure S5: Statistical representation for biological activity for **L**, **Phen** and their metal complexes; Table S1: Selected FT-IR bands for **L**, **Phen** and their metal complexes; Table S2: Maximum temperature (T_{max}, °C) and mass loss of the decomposition steps for **L**, **phen** and metal complexes.

Author Contributions: Conceptualization, M.S.E.-A., S.A.S., H.A.E.-S. and H.M.K.; formal analysis, M.S.E.-A. and H.M.K.; investigation, S.A.S., H.A.E.-S., H.M.K. and H.S.E.; methodology, M.S.E.-A. and H.M.K.; resources, S.A.S.; software, M.S.E.-A. and H.M.K.; supervision, S.A.S. and H.S.E.; validation, S.A.S. and H.S.E.; writing—original draft, M.S.E.-A. and H.A.E.-S.; writing—review and editing, S.A.S. and H.S.E. All authors have read and agreed to the published version of the manuscript.

Funding: This research received no external funding.

Institutional Review Board Statement: Not applicable.

Informed Consent Statement: Not applicable.

Data Availability Statement: Not applicable.

Conflicts of Interest: The authors declare no conflict of interest.

References

1. Boger, D.L.; Weinreb, S.M. *Hetero Diels-Alder Methodology in Organic Synthesis*; Academic Press: Cambridge, MA, USA, 1987. [CrossRef]
2. Tietze, L.F.; Kettschau, G. Hetero Diels-Alder reactions in organic chemistry. *Top. Curr. Chem.* **1997**, *12*, 189. [CrossRef]
3. Grivsky, E.M.; Lee, S.; Sigel, C.W.; Duch, D.S.; Nichol, C.A. Synthesis and antitumor activity of 2,4-diamino-6-(2,5-dimethoxybenzyl)-5-methylpyrido[2,3-d]pyrimidine. *J. Med. Chem.* **1980**, *23*, 327–329. [CrossRef] [PubMed]
4. Broom, A.D.; Shim, J.L.; Anderson, G.L. Pyrido[2,3-d]pyrimidines. IV. Synthetic studies leading to various oxopyrido[2,3-d]pyrimidines. *J. Org. Chem.* **1976**, *41*, 1095–1099. [CrossRef] [PubMed]
5. Heber, D.; Heers, C.; Ravens, U. Positive inotropic activity of 5-amino-6-cyano-1,3-dimethyl-1,2,3,4-tetrahydropyrido[2,3-d]pyrim idine-2,4-dione in cardiac muscle from guinea-pig and man. Part 6: Compounds with positive inotropic activity. *Die Pharm.* **1993**, *48*, 537–541.
6. Asadian, M.; Davoodnia, A.; Beyramabadi, S.A. Efficient Synthesis of New Pyrimido[5′,4′:5,6]pyrano[2,3-d]pyrimidine-2,4,6(1H,3H)-triones via the Tandem Intramolecular Pinner–Dimroth Rearrangement, and Their Antibacterial Activity. *Russ. J. Gen. Chem.* **2018**, *88*, 2658–2663. [CrossRef]
7. Poola, S.; Shaik, M.S.; Sudileti, M.; Yakkate, S.; Nalluri, V.; Chippada, A.; Cirandur, S.R. Nano CuO–Ag-catalyzed synthesis of some novel pyrano[2,3-d] pyrimidine derivatives and evaluation of their bioactivity. *J. Chin. Chem. Soc.* **2020**, *67*, 805–820. [CrossRef]
8. Amininia, A.; Pourshamsian, K.; Sadeghi, B. Nano-ZnO Impregnated on Starch—A Highly Efficient Heterogeneous Bio-Based Catalyst for One-Pot Synthesis of Pyranopyrimidinone and Xanthene Derivatives as Potential Antibacterial Agents. *Russ. J. Org. Chem.* **2020**, *56*, 1279–1288. [CrossRef]
9. Tozkoparan, B.; Ertan, M.; Kelicen, P.; Demirdamar, R. Synthesis and anti-inflammatory activities of some thiazolo[3,2-a]pyrimidine derivatives. *Il Farm.* **1999**, *54*, 588–593. [CrossRef]
10. Agarwal, A.; Srivastava, K.; Puri, S.; Chauhan, P.M. Synthesis of 2,4,6-trisubstituted pyrimidines as antimalarial agents. *Bioorganic Med. Chem.* **2005**, *13*, 4645–4650. [CrossRef]
11. Cerecetto, H.; Di Maio, R.; González, M.; Risso, M.; Sagrera, G.; Seoane, G.; Denicola, A.; Peluffo, G.; Quijano, C.; Stoppani, A.O.; et al. Synthesis and antitrypanosomal evaluation of E-isomers of 5-nitro-2-furaldehyde and 5-nitrothiophene-2-carboxaldehyde semicarbazone derivatives. Structure–activity relationships. *Eur. J. Med. Chem.* **2000**, *35*, 343–350. [CrossRef]
12. Bruno, O.; Brullo, C.; Schenone, S.; Bondavalli, F.; Ranise, A.; Tognolini, M.; Impicciatore, M.; Ballabeni, V.; Barocelli, E. Synthesis, antiplatelet and antithrombotic activities of new 2-substituted benzopyrano[4,3-d]pyrimidin-4-cycloamines and 4-amino/cycloamino-benzopyrano[4,3-d]pyrimidin-5-ones. *Bioorganic Med. Chem.* **2006**, *14*, 121–130. [CrossRef] [PubMed]
13. Chabchoub, F.; Messaâd, M.; Ben Mansour, H.; Chekir-Ghedira, L.; Salem, M. Synthesis and antigenotoxic activity of some naphtho[2,1-b]pyrano[3,2-e][1,2,4]triazolo[1,5-c]pyrimidine derivatives. *Eur. J. Med. Chem.* **2007**, *42*, 715–718. [CrossRef] [PubMed]
14. Fan, X.; Feng, D.; Qu, Y.; Zhang, X.; Wang, J.; Loiseau, P.; Andrei, G.; Snoeck, R.; De Clercq, E. Practical and efficient synthesis of pyrano[3,2-c]pyridone, pyrano[4,3-b]pyran and their hybrids with nucleoside as potential antiviral and antileishmanial agents. *Bioorganic Med. Chem. Lett.* **2010**, *20*, 809–813. [CrossRef] [PubMed]
15. El-Sayed, H.A.; Said, S.A. Direct Synthesis of Multi-functional Pyrimidine, Pyrazine, and Pyridine Scaffolds *via* Inter- and Intramolecular Annulations of 3-Amino-thieno[2,3- *b*]pyridine-2-carboxylate. *J. Heterocycl. Chem.* **2019**, *56*, 1030–1037. [CrossRef]
16. Assy, M.G.; El-Sayed, H.A.; Ouf, N.H.; Hamza, A.; Morsy, H.A. Cycloaddition of Aroyl Isothiocyanate: A Novel Synthesis of Triazine, Oxazine, Pyrimidine, and Pyridine Derivatives. *J. Heterocycl. Chem.* **2019**, *56*, 2954–2959. [CrossRef]
17. El-Sayed, H.A. Design and synthesis of some tricyclic pyrimidines and triazines via cycloaddition and intermolecular cyclization of cyclic amidine. *J. Iran. Chem. Soc.* **2017**, *14*, 2239–2246. [CrossRef]
18. El-Sayed, H.A.; Morsy, H.A. A facile synthesis of highly fluorescent pyrido[2,3-d]pyrimidines and 1,8-naphthyridines via oxazine transformation and enaminic addition reactions. *J. Iran. Chem. Soc.* **2019**, *16*, 723–732. [CrossRef]
19. El-Sayed, H.A.; Hamid, A.M.A.; Assy, M.G.; Faraj, T.S. Intermolecular cyclization of cinnamoyl isothiocyanate: A new synthetic entry for pyrimidine, triazine, and triazole candidates. *Synth. Commun.* **2018**, *48*, 786–794. [CrossRef]
20. Shijay, G.; Cheng, H.T.; Chi, T.; Ching-Fa, Y. Fluoride ion catalyzed multicomponent reactions for efficient synthesis of 4H-chromene and N-arylquinoline derivatives in aqueous media. *Tedrahedron* **2008**, *64*, 9143–9149. [CrossRef]
21. Oskooie, H.A.; Heravi, M.M.; Karimi, N.; Zadeh, M.E. Caro's Acid–Silica Gel: An Efficient and Versatile Catalyst for the One-Pot Synthesis of Tetrahydrobenzo[*b*]pyran Derivatives. *Synth. Commun.* **2011**, *41*, 436–440. [CrossRef]
22. Hafez, E.A.A.; Elnagdi, M.H.; Elagamey, A.G.A.; El-Taweel, F.M.A.A. Nitriles in Heterocyclic Synthesis: Novel Synthesis of Benzo[c]coumarin and of Benzo[c]pyrano[3,2-c]quinoline Derivatives. *Heterocycles* **1987**, *26*, 903–907. [CrossRef]
23. Ellis, G.P. *The Chemistry of Heterocyclic Compounds: Chromenes, Chromanes and Chromones*; Weissberger, A., Taylor, E.C., Eds.; John Wiley: New York, NY, USA, 1977; pp. 11–139.
24. Gao, Y.; Yang, W.; Du, D.M. Efficient organocatalytic asymmetric synthesis of 2-amino-4H-chromene-3-carbonitrile derivatives. *Tetrahedron Asymm.* **2012**, *23*, 339–344. [CrossRef]

25. Reynolds, G.; Drexhage, K. New coumarin dyes with rigidized structure for flashlamp-pumped dye lasers. *Opt. Commun.* **1975**, *13*, 222–225. [CrossRef]
26. Zollinger, H. Color chemistry. In *Syntheses, Properties, and Applications of Organic Dyes and Pigments/Heinrich Zollinger*, 3rd ed.; Verlag Helvetica Chimica Acta; Zurikh and Wiley-VCH: Cambridge, UK, 2003.
27. Bissell, E.R.; Mitchell, A.R.; Smith, R.E. Synthesis and chemistry of 7-amino-4-(trifluoromethyl)coumarin and its amino acid and peptide derivatives. *J. Org. Chem.* **1980**, *45*, 2283–2287. [CrossRef]
28. Khaksar, S.; Rouhollahpour, A.; Talesh, S.M. A facile and efficient synthesis of 2-amino-3-cyano-4H-chromenes and tetrahydrobenzo[b]pyrans using 2,2,2-trifluoroethanol as a metal-free and reusable medium. *J. Fluor. Chem.* **2012**, *141*, 11–15. [CrossRef]
29. Saha, M.; Pal, A.K. Palladium (0) Nanoparticles: A Novel and Reusable Catalyst for the Synthesis of Various Pyran Derivatives. *Adv. Nanoparticles* **2012**, *1*, 61–70. [CrossRef]
30. Abouzid, K.A.; Al-Ansary, G.H.; El-Naggar, A.M. Eco-friendly synthesis of novel cyanopyridine derivatives and their anticancer and PIM-1 kinase inhibitory activities. *Eur. J. Med. Chem.* **2017**, *134*, 357–365. [CrossRef]
31. Sadeek, S.; El-Hamid, S.A. Preparation, characterization and cytotoxicity studies of some transition metal complexes with ofloxacin and 1,10-phenanthroline mixed ligand. *J. Mol. Struct.* **2016**, *1122*, 175–185. [CrossRef]
32. Sadeek, S.A.; El-Hamid, S.M.A. Synthesis, spectroscopic, thermal analysis and in vitro biological properties of some new metal complexes with gemifloxacin and 1,10-phenanthroline. *J. Therm. Anal. Calorim.* **2015**, *124*, 547–562. [CrossRef]
33. Katsarou, M.E.; Efthimiadou, E.K.; Psomas, G.; Karaliota, A.; Vourloumis, D. Novel Copper(II) Complex of *N*-Propyl-norfloxacin and 1,10-Phenanthroline with Enhanced Antileukemic and DNA Nuclease Activities. *J. Med. Chem.* **2008**, *51*, 470–478. [CrossRef]
34. Chen, M.-Z.; Zhou, C.-Q.; Lin, W.-E.; Chen, J.-X.; Chen, W.-H.; Jiang, Z.-H. Synthesis, Crystal Structures and DNA-Cleaving Activities of [Cemp]2[MCl4] (Cemp=N-Carbethoxymethyl-1,10-phenanthrolinium, M = CuII, ZnII, CoII, NiII and MnII). *Chem. Pharm. Bull.* **2013**, *61*, 714–721. [CrossRef] [PubMed]
35. Kharadi, G.J. Molar conductance, magnetic susceptibility, mass spectra, and thermal decomposition studies on Cu(II) compounds with substituted terpyridines and clioquinol drug. *J. Therm. Anal. Calorim.* **2014**, *117*, 333–341. [CrossRef]
36. Bellér, G.; Lente, G.; Fábián, I. Central Role of Phenanthroline Mono-*N*-oxide in the Decomposition Reactions of Tris(1,10-phenanthroline)iron(II) and -iron(III) Complexes. *Inorg. Chem.* **2010**, *49*, 3968–3970. [CrossRef]
37. Singh, C.P.; Singh, A.; Nibha; Daniliuc, C.G.; Kumar, B.; Singh, G. Preparation, crystal structure and thermal studies of cadmium perchlorate complex with 2,2′-bipyridine. *J. Therm. Anal. Calorim.* **2015**, *121*, 633–640. [CrossRef]
38. El-Deen, I.; Shoair, A.; El-Bindary, M. Synthesis, characterization and biological properties of oxovanadium(IV) complexes. *J. Mol. Struct.* **2019**, *1180*, 420–437. [CrossRef]
39. Sahyon, H.; El-Bindary, A.; Shoair, A.; Abdellatif, A. Synthesis and characterization of ruthenium(III) complex containing 2-aminomethyl benzimidazole, and its anticancer activity of in vitro and in vivo models. *J. Mol. Liq.* **2018**, *255*, 122–134. [CrossRef]
40. Shoair, A.; El-Bindary, A.; El-Ghamaz, N.; Rezk, G. Synthesis, characterization, DNA binding and antitumor activities of Cu(II) complexes. *J. Mol. Liq.* **2018**, *269*, 619–638. [CrossRef]
41. Sadeek, S.A.; El-Hamid, S.M.A.; Mohamed, A.A.; Zordok, W.A.; El-Sayed, H.A. Spectroscopic characterization, thermogravimetry, density functional theory and biological studies of some mixed-ligand complexes of meloxicam and 2,2′-bipyridine with some transition metals. *Appl. Organomet. Chem.* **2019**, *33*, e4889. [CrossRef]
42. Elshafie, H.S.; Sakr, S.H.; Sadeek, S.A.; Camele, I. Biological Investigations and Spectroscopic Studies of New Moxifloxacin/Glycine-Metal Complexes. *Chem. Biodivers.* **2019**, *16*, e1800633. [CrossRef]
43. Abd El-Hamid, S.M.; Sadeek, S.A.; Zordok, W.A.; El-Shwiniy, W.H. Synthesis, spectroscopic studies, DFT calculations, cytotoxicity and antimicrobial activity of some metal complexes with ofloxacin and 2,2′-bipyridine. *J. Mol. Struct.* **2019**, *1176*, 422–433. [CrossRef]
44. El-Hamid, S.M.A.; Sadeek, S.A.; Mohammed, S.F.; Ahmed, F.M.; El-Gedamy, M.S. N_2O_2-chelate metal complexes with Schiff base ligand: Synthesis, characterisation and contribution as a promising antiviral agent against human cytomegalovirus. *Appl. Organomet. Chem.* **2023**, *37*, e6958. [CrossRef]
45. Geary, W.J. The use of conductivity measurements in organic solvents for the characterisation of coordination compounds. *Co-ord. Chem. Rev.* **1971**, *7*, 81–122. [CrossRef]
46. El-Shwiniy, W.; Sadeek, S. Synthesis and characterization of new 2-cyano-2-(p-tolyl-hydrazono)-thioacetamide metal complexes and a study on their antimicrobial activities. *Spectrochim. Acta Part A Mol. Biomol. Spectrosc.* **2015**, *137*, 535–546. [CrossRef] [PubMed]
47. Zordok, W.; Sadeek, S. Synthesis, spectroscopic characterization, biological studies and DFT calculations on some transition metal complexes of NO donor ligand. *J. Mol. Struct.* **2018**, *1158*, 205–220. [CrossRef]
48. Mayr, A.; Mao, L.F. Cyanoisocyanoarene Metal Complexes as Building Blocks for Coordination Polymers: Structural Nonrigidity of a Metal−Nitrile Linkage[1]. *Inorg. Chem.* **1998**, *37*, 5776–5780. [CrossRef]
49. Cordiner, R.L.; Jove´, D.A.; Roberts, R.L.; Farmer, J.D.; Puschmann, H.; Corcoran, D.; Goeta, A.E.; Howard, J.A.K.; Low, P.J. Syntheses and molecular structures of group 8 benzonitrile complexes. *J. Organomet. Chem.* **2005**, *690*, 4908–4919. [CrossRef]
50. Li, Y.; Chai, Y.; Yuan, R.; Liang, W. Synthesis and application of a new copper(II) complex containing oflx and leof. *Russ. J. Inorg. Chem.* **2008**, *53*, 704–706. [CrossRef]
51. Nakamoto, K. *Infrared and Raman Spectra of Inorganic and Coordination Compounds*, 4th ed.; Wiley: New York, NY, USA, 1986; p. 230.

52. Mohamed, A.A.; Nassr, A.A.; Sadeek, S.A.; Elshafie, H.S. Synthesis and Spectral, Thermal and Antimicrobial Investigation of Mixed Ligand Metal Complexes of *N*-Salicylidene Aniline and 1,10-Phenanthroline. *Compounds* **2023**, *3*, 298–309. [CrossRef]
53. Kamal, H.M.; El-Sayed, H.A.; Sadeek, S.A.; Zordok, W.A.-A.; El-Attar, M.S. Spectroscopic characterization, DFT modeling and antimicrobial studies of some novel nanoparticles mixed ligand complexes of NS bidentate ligand in presence of 2,2′-bipyridine. *J. Mol. Liq.* **2023**, *376*, 121404. [CrossRef]
54. Almond, M.J.; Redman, H.; Rice, D.A. Growth of thin layers of metal sulfides by chemical vapour deposition using dual source and single source precursors: Routes to Cr_2S_3, α-MnS and FeS. *J. Mater. Chem.* **2000**, *10*, 2842–2846. [CrossRef]
55. Yousef, T.; Abu El-Reash, G.; Rakha, T.; El-Ayaan, U. First row transition metal complexes of (E)-2-(2-(2-hydroxybenzylidene) hydrazinyl)-2-oxo-N-phenylacetamide complexes. *Spectrochim. Acta Part A Mol. Biomol. Spectrosc.* **2011**, *83*, 271–278. [CrossRef] [PubMed]
56. Lehmann, U.; Lach, J.; Loose, C.; Hahn, T.; Kersting, B.; Kortus, J. Binuclear nickel complexes with an edge sharing bis(square-pyramidal) $N_3Ni(\mu\text{-}S_2)NiN_3$core: Synthesis, characterization, crystal structure and magnetic properties. *Dalton Trans.* **2013**, *42*, 987–996. [CrossRef] [PubMed]
57. Sathyadevi, P.; Krishnamoorthy, P.; Jayanthi, E.; Butorac, R.R.; Cowley, A.H.; Dharmaraj, N. Studies on the effect of metal ions of hydrazone complexes on interaction with nucleic acids, bovine serum albumin and antioxidant properties. *Inorganica Chim. Acta* **2012**, *384*, 83–96. [CrossRef]
58. Elshafie, H.S.; Sadeek, S.A.; Camele, I.; Mohamed, A.A. Biochemical Characterization of New Gemifloxacin Schiff Base (GMFX-o-phdn) Metal Complexes and Evaluation of Their Antimicrobial Activity against Some Phyto- or Human Pathogens. *Int. J. Mol. Sci.* **2022**, *23*, 2110. [CrossRef] [PubMed]
59. Coats, A.W.; Redfern, J.P. Kinetic Parameters from Thermogravimetric Data. *Nature* **1964**, *201*, 68–69. [CrossRef]
60. Horowitz, H.H.; Metzger, G. A New Analysis of Thermogravimetric Traces. *Anal. Chem.* **1963**, *35*, 1464–1468. [CrossRef]
61. Rahmouni, N.T.; Bensiradj, N.E.H.; Megatli, S.A.; Djebbar, S.; Baitich, O.B. New mixed amino acids complexes of iron(III) and zinc(II) with isonitrosoacetophenone: Synthesis, spectral characterization, DFT study and anticancer activity. *Spectrochim. Acta Part A Mol. Biomol. Spectrosc.* **2019**, *213*, 235–248. [CrossRef]
62. Moore, J.W.; Pearson, R.G. *Kinetic and Mechanism*; John Wiley & Sons: New York, NY, USA, 1981.
63. Ilhan, S.; Temel, H.; Yilmaz, I.; Şekerci, M. Synthesis and characterization of new macrocyclic Schiff base derived from 2,6-diaminopyridine and 1,7-bis(2-formylphenyl)-1,4,7-trioxaheptane and its Cu(II), Ni(II), Pb(II), Co(III) and La(III) complexes. *Polyhedron* **2007**, *26*, 2795–2802. [CrossRef]
64. Al-Amiery, A.A.; Al-Majedy, Y.K.; Ibrahim, H.H.; Al-Tamimi, A.A. Antioxidant, antimicrobial, and theoretical studies of the thiosemicarbazone derivative Schiff base 2-(2-imino-1-methylimidazolidin-4-ylidene)hydrazinecarbothioamide (IMHC). *Org. Med. Chem. Lett.* **2012**, *2*, 4. [CrossRef]
65. Khan, M.; Khan, A.; Hussain, I.; Gul, S.; Iqbal, M.; Rahman, I.U.; Khuda, F. Spectral, XRD, SEM and biological properties of new mononuclear Schiff base transition metal complexes. *Inorg. Chem. Commun.* **2013**, *35*, 104–109. [CrossRef]
66. El-Bindary, A.; El-Sonbati, A.; Diab, M.; Morgan, S. Geometrical structure, potentiometric and thermodynamic studies of rhodanine azodye and its metal complexes. *J. Mol. Liq.* **2014**, *201*, 36–42. [CrossRef]
67. Abu-Eittah, R.H.; Zordok, W.A. A molecular orbital treatment of piroxicam and its M2+-complexes: The change of the drug configuration in a time of bond formation. *J. Mol. Struct. THEOCHEM* **2010**, *951*, 14–20. [CrossRef]
68. Defazio, S.; Cini, R. Synthesis, X-ray structure and molecular modelling analysis of cobalt(ii), nickel(ii), zinc(ii) and cadmium(ii) complexes of the widely used anti-inflammatory drug meloxicam. *J. Chem. Soc. Dalton Trans.* **2002**, *9*, 1888–1897. [CrossRef]
69. Wang, X.; Ren, Q.; Fan, H.; Chen, J.; Sun, Z.; Li, T.; Liu, X.; Zhang, G.; Xu, D.; Liu, W. Preparation, crystal structure, spectrographic characterization, thermal and third order nonlinear optical properties of benzyltriethylamine bis(2-thioxo-1,3-dithiole-4,5-dithiolato)nickel(III). *J. Cryst. Growth* **2010**, *312*, 2206–2214. [CrossRef]
70. Altürk, S.; Avcı, D.; Başoğlu, A.; Tamer, Ö.; Atalay, Y.; Dege, N. Copper(II) complex with 6-methylpyridine-2-carboxyclic acid: Experimental and computational study on the XRD, FT-IR and UV–Vis spectra, refractive index, band gap and NLO parameters. *Spectrochim. Acta Part A Mol. Biomol. Spectrosc.* **2018**, *190*, 220–230. [CrossRef]
71. El-Sayed, A.S.A.; Shindia, A.A.; Zeid, A.A.A.; Yassin, A.M.; Sitohy, M.Z.; Sitohy, B. Aspergillus nidulans thermostable arginine deiminase-Dextran conjugates with enhanced molecular stability, proteolytic resistance, pharmacokinetic properties and anticancer activity. *Enzym. Microb. Technol.* **2019**, *131*, 109432. [CrossRef]
72. El-Sayed, A.S.A.; Abdel-Azeim, S.; Ibrahim, H.M.; Yassin, M.A.; Abdel-Ghany, S.E.; Esener, S.; Ali, G.S. Biochemical stability and molecular dynamic characterization of Aspergillus fumigatus cystathionine γ-lyase in response to various reaction effectors. *Enzym. Microb. Technol.* **2015**, *81*, 31–46. [CrossRef]
73. Zhao, P.; Shangguan, R.; Wang, H.; Qing, Y.; Jian, F. Synthesis, characterization, crystal structure and ab initio studies on 5-ethoxycarbonly-6-methyl-4-phenyl-2-thioxo-1,2,3,4-tetrahydropyrimidine. *Spectrochim. Acta Part A Mol. Biomol. Spectrosc.* **2009**, *72*, 61–67. [CrossRef]
74. Andruh, M.; Melanson, R.; Stager, C.V.; Rochon, F.D. $[Cr(bipy)(C_2O_4)_2]^-$—A versatile building block for the design of heteropolymetallic systems 2. Syntheses and crystal structures of CuCr2(bipy)2$(\mu\text{-}C_2O_4)_4(C_2O_4)_4(H_2O)_2\cdot 112H_2O$ and $(AgCr(bipy)(\mu\text{-}C_2O_4)_2(H_2O)_2)_2$ and magnetic properties of the copper(II) derivative. *Inorganica Chim. Acta* **1996**, *251*, 309–317. [CrossRef]

75. Anderson, R.A.; Cheng, N.; A. Bryden, N.; Polansky, M.M.; Cheng, N.; Chi, J.; Feng, J. Elevated Intakes of Supplemental Chromium Improve Glucose and Insulin Variables in Individuals with Type 2 Diabetes. *Diabetes* **1997**, *46*, 1786–1791. [CrossRef] [PubMed]
76. Bassett, J.; Denney, R.C.; Jeffery, G.H.; Mendham, J. *Vogel's Textbook of Quantitative Inorganic Analysis Including Elementary Instrumental Analysis*, 4th ed.; Longman Group: London, UK, 1978.
77. Lewis, J.; Wilkins, R.G. *Modern Coordination Chemistry*; Interscience: New York, NY, USA, 1960; pp. 403–406.
78. El-Sayed, H.A.; Said, S.A.; El-Hamid, A.A.; Mohamed, A.S.A.; Amr, A.E.; Morsy, H.A. Functionalization of Ethyl 6-Amino-4-(4-chlorophenyl)-5-cyano-2-methyl-4H-pyran-3-carboxylate: Facile Synthesis of a New Series of Pyrano[2,3-d]pyrimidine Derivatives. *Russ. J. Gen. Chem.* **2021**, *91*, 1403–1408. [CrossRef]
79. Lalhruaizela; Marak, B.N.; Sran, B.S.; Singh, V.P. Multicomponent Synthesis, Crystal Structure, Hirshfeld Surface Analysis, and Molecular Docking of 4H-Pyrans. *Chemistryselect* **2021**, *6*, 11249–11260. [CrossRef]
80. Beecher, D.J.; Wong, A.C.L. Identification of Hemolysin BL-Producing Bacillus cereus Isolates by a Discontinuous Hemolytic Pattern in Blood Agar. *Appl. Environ. Microb.* **1994**, *60*, 1646–1651. [CrossRef]
81. Elshafie, H.S.; Sakr, S.; Bufo, S.A.; Camele, I. An Attempt of Biocontrol the Tomato-Wilt Disease Caused by *Verticillium dahliae* Using *Burkholderia gladioli* pv. agaricicola and Its Bioactive Secondary Metabolites. *Int. J. Plant Biol.* **2017**, *8*, 57–60. [CrossRef]
82. Elshafie, H.S.; Viggiani, L.; Mostafa, M.S.; El-Hashash, M.; Camele, I.; Bufo, S.A. Biological activity and chemical identification of ornithine lipid produced by *Burkholderia gladioli* pv. agaricicola ICMP 11096 using LC-MS and NMR analyses. *J. Biol. Res. Boll. Soc. Ital. Biol. Sper.* **2017**, *90*, 96–103. [CrossRef]
83. Casey, J.; O'Cleirigh, C.; Walsh, P.; O'Shea, D. Development of a robust microtiter plate-based assay method for assessment of bioactivity. *J. Microbiol. Methods* **2004**, *58*, 327–334. [CrossRef]